J|A|C|S ARTICLES

Published on Web 03/12/2010

Concurrent Synergism and Inhibition in Bimetallic Catalysis: Catalytic Binuclear Elimination, Solute−Solute Interactions and a Hetero-Bimetallic Hydrogen-Bonded Complex in Rh−Mo Hydroformylations

Chuanzhao Li,* Shuying Cheng, Martin Tjahjono, Martin Schreyer, and Marc Garland*

*Institute of Chemical and Engineering Sciences, A*STAR (Agency for Science, Technology and Research), 1 Pesek Road, Jurong Island, Singapore, 627833*

Received March 19, 2009; E-mail: marc_garland@ices.a-star.edu.sg; li_chuanzhao@ices.a-star.edu.sg

Abstract: Hydroformylations of cyclopentene and 3,3-dimethylbut-1-ene were performed using both $Rh_4(CO)_{12}$ and $(\eta^5\text{-}C_5H_5)Mo(CO)_3H$ as precursors in *n*-hexane at 298 K. Both stoichiometric and catalytic hydroformylations were conducted as well as isotopic labeling experiments. Six organometallic pure component spectra were recovered from the high-pressure FTIR experiments, namely the known species $Rh_4(CO)_{12}$, $(\eta^5\text{-}C_5H_5)Mo(CO)_3H$, $RCORh(CO)_4$, and the new heterobimetallic complexes $RhMo(CO)_7(\eta^5\text{-}C_5H_5)$, a weak hydrogen bonded species $(\eta^5\text{-}C_5H_5)Mo(CO)_3H-C_5H_9CORh(CO)_4$, and a substituted $RhMo(CO)_{7\text{-}y}(\eta^5\text{-}C_5H_5)L_y$, where $y = 1$ or 2 and $L = (\pi\text{-}C_5H_8)$. The main findings were (1) catalytic binuclear elimination (CBER) occurs between $(\eta^5\text{-}C_5H_5)Mo(CO)_3H$ and $RCORh(CO)_4$ resulting in aldehyde and $RhMo(CO)_7(\eta^5\text{-}C_5H_5)$, and this mechanism is responsible for ca. 10% of the product formation; (2) molecular hydrogen is readily activated by the new heterobimetallic complex(es); (3) FTIR and DFT spectroscopic evidence suggests that the weak hydrogen bonded species $(\eta^5\text{-}C_5H_5)Mo(CO)_3H-C_5H_9CORh(CO)_4$ has an interaction of the type $\eta^5\text{-}C_5H_4-H\cdots O{=}C$; and (4) independent physicochemical experiments for volumes of interaction confirm that significant solute−solute interactions are present. With respect to the efficiency of the catalytic cycle, the formation of a weak $(\eta^5\text{-}C_5H_5)Mo(CO)_3H-C_5H_9CORh(CO)_4$ complex results in a significant decrease in the measured turnover frequency (TOF) and is the primary reason for the inhibition observed in the bimetallic catalytic hydroformylation. Such hydrogen bonding through the $\eta^5\text{-}C_5H_5$ ring might have relevance to inhibition observed in other catalytic metallocene systems. The present catalytic system is an example of concurrent *synergism* and *inhibition* in bimetallic homogeneous catalysis.

Introduction

Various mechanisms can be responsible for deactivation in transition-metal homogeneous catalyzed systems.[1] Some of the more dramatic changes such as ligand degradation, that is, phosphine oxidation and intrametalation,[2] reduction of complexes to metal,[3] reactions with impurities to form ultrastable and nonlabile species,[4] etc. are relatively well understood, and in some cases, preventative action can be taken.[5] However, more subtle inhibition in homogeneous catalyzed systems is certainly less understood. Some undesirable changes might be induced by relatively weak solute−solute interactions, such as hydrogen bonding, ion-pairing, dipole−dipole interactions, etc.[6] The detection of subtle deactivation phenomenon, as well as the confirmation of relatively weak solute−solute interactions, represents a significant challenge. Moreover, detailed understanding of these effects would surely provide new opportunities and directions for research in homogeneous catalysis.

In the past two decades, in situ spectroscopic methods have been increasingly applied to transition-metal homogenously catalyzed reactions.[7] This has resulted in a considerably better mechanistic understanding of many systems, by facilitating the identification of new chemistry and intermediates[8] and allowing

(1) Detlef, H.; de Vries, A. H. M.; de Vries, J. G. In *Handbook of Homogeneous Hydrogenation*; de Vries, J. G., Cornelis, J., Eds.; Elsevier VCH: New York, 2007; Vol. 3, pp 1483−1516.
(2) (a) Garrou, P. E. *Chem. Rev.* **1985**, *85* (3), 171–185. (b) Parshall, G. W.; Knoth, W. H.; Schunn, R. A. *J. Am. Chem. Soc.* **1969**, *91* (18), 4990–4995. (c) Hage, R.; Iburg, J. E.; Kerschner, J.; Koek, J. H.; Lempers, E. L. M.; Martens, R. J.; Racherla, U. S.; Russell, S. W.; Swarthoff, T.; van Vliet, M. R. P.; Warnaar, J. B.; Wolf, L. V. D.; Krijnen, B. *Nature* **1994**, *369* (6482), 637–639. (d) Collins, T. J. *Acc. Chem. Res.* **1994**, *27* (9), 279–285. (e) Horwitz, C. P.; Fooksman, D. R.; Vuocolo, L. D.; Gordon-Wylie, S. W.; Cox, N. J.; Collins, T. J. *J. Am. Chem. Soc.* **1998**, *120* (19), 4867–4868. (f) Kong, K. C.; Cheng, C. H. *J. Am. Chem. Soc.* **1991**, *113* (16), 6313–6315. (g) Van Leeuwen, P. W. N. M.; Roobeek, C. F.; Orpen, A. G. *Organometallics* **1990**, *9* (8), 2179–2181.
(3) Lewis, L. N. *J. Am. Chem. Soc.* **1990**, *112* (16), 5998–6004.
(4) Walczuk, E. B.; Kamer, P. C. J.; van Leeuwen, P. W. N. M. *Angew. Chem., Int. Ed.* **2003**, *42* (38), 4665–4669.
(5) van Leeuwen, P. W. N. M. *Appl. Catal., A: Gen.* **2001**, *212* (1−2), 61–81.
(6) (a) Cesarotti, E.; Ugo, R.; Kaplan, L. *Coord. Chem. Rev.* **1982**, *43*, 275–98. (b) Huang, Y.; Rawal, H. *J. Am. Chem. Soc.* **2002**, *124*, 9662–9663. (c) Breit, B.; Seiche, W. *J. Am. Chem. Soc.* **2003**, *125*, 6608–6609. (d) Fulton, J. R.; Holland, A. W.; Fox, D. J.; Bergman, R. G. *Acc. Chem. Res.* **2002**, *35*, 44–56. (e) Casey, C. P.; Clark, T. B.; Guzai, A. *J. Am. Chem. Soc.* **2007**, *129*, 11821–11827.

the evaluation of detailed kinetics and turnover frequencies.[9] In addition, advances in signal processing and chemometric techniques have significantly improved the limits of detection.[10] Although these developments have largely focused on understanding the primary characteristics of quite active catalytic systems, potential certainly exists for using these tools to better understand more subtle aspects of the chemistry, for example changes in selectivity and activity patterns.

Bimetallic and multimetallic homogeneous catalyzed reactions have attracted considerable attention, due in part to dramatically increased reaction rates observed in some systems.[11] The mechanistic basis for synergism has been clearly identified for a few systems using in situ spectroscopic techniques. These include (1) the Ir/Ru catalyzed carbonylation of methanol, where NMR has shown that Ru aids in the abstraction of iodine from a crucial iridium intermediate,[12] and (2) the Rh/Mn and Rh/Re hydroformylations of alkenes, where in situ FTIR has shown that catalytic binuclear elimination occurs.[9d,e,g,h,13]

In the present contribution, the hydroformylation of cyclopentene and 3,3-dimethylbut-1-ene starting with $Rh_4(CO)_{12}$ and $(\eta^5\text{-}C_5H_5)Mo(CO)_3H$ as catalyst precursors was performed, and in situ FTIR was used as the quantitative spectroscopic method. In this heterobimetallic system, both synergistic and inhibitory effects were observed. Consequently, stoichiometric and labeling experiments were performed to clarify mechanistic issues, particularly the presence of catalytic binuclear elimination. The spectroscopic, kinetic, and physicochemical measurements together with DFT calculations confirm that solute−solute interactions are occurring, in particular hydrogen bonding, and that these interactions are responsible for the inhibitory effects on the catalytic cycle.

Experimental Section

General. All solution preparations and transfers were carried out under purified argon (99.9995%, Saxol, Singapore) atmosphere using standard Schlenk techniques or conducted in a glovebox (especially when handling $(\eta^5\text{-}C_5H_5)Mo(CO)_3H$). The argon was further purified before use by passing it through a deoxy and zeolite packed column. Carbon monoxide (research grade, 99.97%, Saxol, Singapore), hydrogen (99.9995%, Saxol, Singapore), and deuterium (99.8%, Spectra Gases, Branchburg, NJ) were also further purified through deoxy and zeolite columns before they were used in the hydroformylation experiments. Purified air was used to purge the Bruker Vertex70 FT-IR spectrometer system.

The chemicals used in the present study include *n*-hexane (99.5% Fluka puriss), $Rh_4(CO)_{12}$ (98% Strem), and $(\eta^5\text{-}C_5H_5)Mo(CO)_3H$ (Sigma Aldrich), cyclopentene (99%, Fluka), 3,3-dimethylbut-1-ene (99%, Fluka, 33DMB), and cyclopentane carboxaldehyde. The *n*-hexane was purified by distillation from NaK under argon. The cyclopentene was purified by distillation from maleic anhydride to remove dienes, followed by distillation from CaH_2 under argon.[9e] The organometallics $Rh_4(CO)_{12}$ and $(\eta^5\text{-}C_5H_5)Mo(CO)_3H$ were used without further purification.

Apparatus. Hydroformylations were performed in an in-house designed 100 mL high-pressure SS316 reactor, which was connected with an injection block, and a high-pressure magnetically driven gear pump (Model GAH-X21, Micro pump, Vancouver, WA). The high-pressure infrared cell was situated in a Bruker Vertex-70 FT-IR spectrometer, and the spectral resolution was 2 cm^{-1} with an interval of 0.12 cm^{-1} for the range 1000−2500 cm^{-1}. A detailed description of the reactor, pump, injection block and mass transfer issues can be found elsewhere.[14] In addition, a high-pressure syringe pump (PHD 4400, Harvard Apparatus) was used for injecting $(\eta^5\text{-}C_5H_5)Mo(CO)_3H$/*n*-hexane under high-pressure reaction conditions. Examples of the use of this experimental system can be found elsewhere,[9] and further details concerning the present experimental setup can be found in the Supporting Information.

In-Situ Spectroscopic and Kinetic Measurements. All of the catalytic hydroformylation experiments were performed in a similar manner. First, a background spectrum of the IR sample chamber was recorded. $Rh_4(CO)_{12}$ and/or $(\eta^5\text{-}C_5H_5)Mo(CO)_3H$ were dissolved in 50 mL of *n*-hexane and then transferred under argon to the reactor. Under 0.2 MPa CO pressure, infrared spectra of the solution in the high-pressure cell were recorded. The total system pressure was raised to 1.7 MPa CO, and the stirrer and high-pressure gear pump were started. After equilibration, infrared spectra of the solution in the high-pressure cell were recorded. Then 1 mL of cyclopentene was injected via the injection block and 1.7 MPa hydrogen was added to start the reactions. The experimental design is listed in Table 1. The high-pressure syringe pump was used for injecting $(\eta^5\text{-}C_5H_5)Mo(CO)_3H$/*n*-hexane in semibatch Exp 5 at ca. 160 min. Spectra were recorded at 1 min intervals in the range 1000−2500 cm^{-1}. In every 4-h experiment, ca. 250 spectra were taken. Note that the gas pressures were changed in Exp 7−9 to promote a higher yield of $RCORh(CO)_4$ for the stoichiometric and labeled experiments.

Volume of Interaction Measurements. Recently, a method has been developed to determine the volumes of interaction between solutes in dilute multicomponent solutions.[15] This method was applied to the present system, during low-pressure noncatalytic conditions, to determine the degree of interaction present in

(7) (a) Laurenczy, G.; Helm, L. In *Mechanisms in Homogeneous Catalysis: A Spectroscopic Approach*; Heaton, B., Ed.; Wiley: Germany, 2005; pp 81−106. (b) Haynes, A. In *Mechanisms in Homogeneous Catalysis: A Spectroscopic Approach*; Heaton, B., Ed.; Wiley: Germany, 2005; pp 107−150. (c) Viviente, E. M.; Pregosin, P. S.; Schott, D. In *Mechanisms in Homogeneous Catalysis: A Spectroscopic Approach*; Heaton, B., Ed.; Wiley: Germany, 2005; pp 1−80. (d) Casey, C. P.; Beetner, S. E.; Johnson, J. B. *J. Am. Chem. Soc.* **2008**, *130*, 2285–2295.

(8) (a) Liu, J.; Heaton, B.; Iggo, J. A.; Whyman, R. *Angew. Chem., Int. Ed.* **2004**, *43* (1), 90–94. (b) Haynes, A.; et al. *J. Am. Chem. Soc.* **2004**, *126*, 2847–2861.

(9) (a) Garland, M.; Pino, P. *Organometallics* **1990**, *10*, 1693–1704. (b) Liu, G.; Volken, R.; Garland, M. *Organometallics* **1999**, *18*, 3429–3436. (c) Feng, J.; Garland, M. *Organometallics* **1999**, *18* (3), 417–427. (d) Li, C.; Widjaja, E.; Garland, M. *J. Am. Chem. Soc.* **2003**, *125*, 5540–5548. (e) Li, C.; Widjaja, E.; Garland, M. *Organometallics* **2004**, *23*, 4131–4138. (f) Liu, G.; Li, C.; Guo, L.; Garland, M. *J. Catal.* **2006**, *237*, 67–78. (g) Li, C.; Chen, L.; Garland, M. *J. Am. Chem. Soc.* **2007**, *129*, 133327–13334. (h) Li, C.; Chen, L.; Garland, M. *Adv. Synth. Catal.* **2008**, *350*, 679–690.

(10) Garland, M. In *Mechanisms in Homogeneous Catalysis: A Spectroscopic Approach*; Heaton, B., Ed.; Wiley: Germany, 2005; pp 151−193.

(11) (a) Guo, N.; Stern, C. L.; Marks, T. J. *J. Am. Chem. Soc.* **2008**, *130* (7), 2246–2261. (b) Sammis, G. M.; Danjo, H.; Jacobsen, E. N. *J. Am. Chem. Soc.* **2004**, *126* (32), 9928–9929. (c) Li, H.; Marks, T. J. *Proc. Natl. Acad. Sci. U.S.A.* **2006**, *103* (42), 15295–15302. (d) Adams, R. D., Albert Cotton, F., Eds. *Catalysis by di-and polynuclear metal cluster complexes*; Wiley: New York, 1998.

(12) (a) Sunley, G. J.; Watson, D. J. *Catal. Today* **2000**, *58*, 293–307. (b) Whyman, R.; Wright, A. P.; Iggo, J. A.; Heaton, B. T. *J. Chem. Soc., Dalton Trans.* **2002**, 771–777.

(13) (a) Collman, J. P.; Hegedus, L. S.; Norton, J. R.; Finke, R. G. *Principles and Applications of Organotransition Metal Chemistry*; University Science Books: Mill Valley, CA, 1987. (b) Norton, J. R. *Acc. Chem. Res.* **1979**, *12*, 139–145. (c) Jones, W. D.; Huggins, J.; Bergman, R. G. *J. Am. Chem. Soc.* **1981**, *103*, 4415–4423. (d) Martin, B.; Warner, D. K.; Norton, J. R. *J. Am. Chem. Soc.* **1986**, *108* (1), 33–39. (e) Nappa, M. J.; Santi, R.; Halpern, J. *Organometallics* **1985**, *4*, 34–41.

(14) Gao, F.; Ng, K.; Li, C.; Krummel, K.; Allian, A.; Garland, M. *J. Catal.* **2006**, *237*, 49–57.

(15) (a) Tjahjono, M.; Guo, L.; Garland, M. *Chem. Eng. Sci.* **2005**, *60* (12), 3239–3249. (b) Tjahjono, M.; Garland, M. *Chem. Eng. Sci.* **2007**, *62*, 3861–3867.

Table 1. Experimental Design for Rh/Mo Hydroformylations of Cyclopentene (CP) and 3,3-Dimethylbut-1-ene (33DMB)

exp no	$Rh_4(CO)_{12}$ loading (mg)	$(\eta^5\text{-}C_5H_5)Mo(CO)_3H$ loading (mg)	Mo/Rh ratio	CO (MPa)	H_2 (MPa)	alkene	*T* (K)
1	14.5	0	0	1.7	1.7	CP	298
2	14.0	15.0	0.82	1.7	1.7	CP	298
3	14.0	25.0	1.36	1.7	1.7	CP	298
4	15.0	37.0	1.88	1.7	1.7	CP	298
5	14.7	35.0[a]	1.82	1.7	1.7	CP	298
6	0	35.0	–	1.7	1.7	CP	298
7	20.1	60.5	2.29	2.7	0, 1.0[b]	CP	298
8	14.6	52.7	2.75	2.7	0, 1.0[c]	CP	298
9	20.2	45.2[d]	1.71	2.8	1.2 (D_2)[d]	33DMB	298

[a] $(\eta^5\text{-}C_5H_5)Mo(CO)_3H$ was added at ca. 160 min. [b] Stoichiometric hydroformylation was carried out initially, and then H_2 was added at ca. 270 min. [c] Stoichiometric hydroformylation was carried out initially, and then H_2 was added at ca. 280 min. [d] Rhodium catalyzed deutero-formylation was carried out initially, then $(\eta^5\text{-}C_5H_5)Mo(CO)_3H$ was added at ca. 320 min.

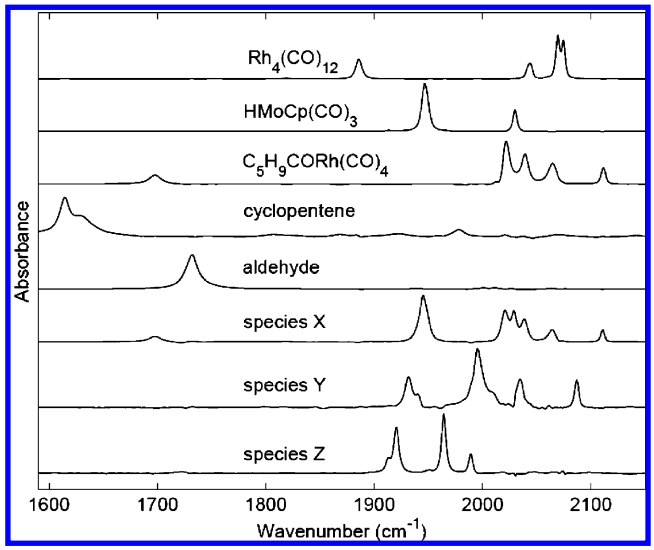

Figure 1. BTEM spectral estimates of the primary observable solutes during the mixed-metal Rh−Mo hydroformylations of cyclopentene. Note that species Y and Z only appeared under stoichiometric conditions in Exp 7−8.

solutions of $(\eta^5\text{-}C_5H_5)Mo(CO)_3H$ and aldehyde. Details of the experiments and the data are provided in the Supporting Information.

Computational Section

Pure Component Spectra, Concentrations, TOF. The in situ reaction spectra were consolidated to give a single absorbance matrix. The spectra were then subjected to singular value decomposition (SVD). The basis vectors were transformed into pure component spectral estimates using the Band-Target Entropy Minimization (BTEM) algorithm.[16] Full-range BTEM spectral estimates are presented (i.e., Figure 1), as well as partial-range BTEM spectral estimates (i.e., Figures 6 and 8), to better resolve the band shifts occurring and reduce artifacts/colinearities. The moles of alkene, aldehyde, $RCORh(CO)_4$, $Rh_4(CO)_{12}$, and $(\eta^5\text{-}C_5H_5)Mo(CO)_3H$ for all experiments could be obtained using a multiple linear regression/least-squares approach using the pure absorptivities. The mathematical procedures have been discussed in detail elsewhere.[10]

The appropriateness of various finite difference schemes for the evaluation of in situ homogeneous catalytic rate data and TOF evaluation has been carefully evaluated.[17] The rates of the product formation of cyclopentane carboxaldehyde were calculated in terms of turn over frequency (TOF) by using eq 1.

$$\mathrm{TOF}_t = \frac{\mathrm{d[aldehyde]}_t/\mathrm{d}t}{[C_5H_9CORh(CO)_4]_t} \qquad (1)$$

Volume of Interactions. The investigation of solute−solute interaction via volumetric measurements involved 4 steps: (1) application of a linear-bilinear response-surface model for the total volume;[15] (2) determinations of volumetric standard states, namely partial molar volumes for solutes at infinite dilution and pure molar volume of the solvent; (3) application of an excess volumetric model based on the McMillan−Mayer theory of solutions; and (4) calculation of the homotactic and heterotactic interaction volumetric coefficients using multilinear regression and validation of the obtained coefficients using statistical tests. The details of the above-mentioned procedure can be found elsewhere.[15]

DFT Calculations. All DFT calculations were performed with Gaussian 03 at the DFT/PBEPBE level. DFT computations were carried out in *n*-heptane solvent using the SCRF model IEFPCM. The organic molecule cyclopentane carboxaldehyde was modeled at the PBEPBE/6-31G (d, p) level. The effective core potentials (ECP) basis set was used to represent the innermost electrons of the molybdenum and rhodium atoms, and the basis set of double-ζ LANL2DZ was employed for molybdenum and rhodium atoms. The basis set of 6-31G(d, p) was used to model the carbon and hydrogen atoms of the Cp rings and carbon, oxygen atoms of carbonyl groups in the $(\eta^5\text{-}C_5H_5)Mo(CO)_3H$, $C_5H_9CORh(CO)_4$, and the associated hydrogen bonded complexes. The basis function 6-311G (d, p) was used for metal-bound hydrogen. The present study takes a similar computational approach, using the same level of theory and basis sets, as previously used to understand intermolecular hydrogen bonding in systems containing metallocenes, and particularly $(\eta^5\text{-}C_5H_5)Mo(CO)_3H$.[18] The optimized geometries and parameters as well as free energies can be found in the Supporting Information.

Results

Pure Component Spectra. BTEM analysis of the entire set of experimental in situ FTIR hydroformylation (Exp 1−8) spectra provided spectral estimates for the hexane solvent, dissolved CO, as well as the observable organic and organometallic solutes present. Figure 1 shows the spectral estimates for the precursors $Rh_4(CO)_{12}$ and $(\eta^5\text{-}C_5H_5)Mo(CO)_3H$, the organics cyclopentene and cyclopentane carboxaldehyde, as well as an intermediate $C_5H_9CORh(CO)_4$ and three new species X, Y, and Z. The species X has vibrational maxima at 2111, 2064. 2038.5, 2029, 2020.5, 1945, and 1700 (broad) cm^{-1}. The other two species Y and Z were only observed in the stoichiometric experiments. Species Y has vibrations at 2086, 2034, 2010, 1996, 193,1 and 1940 (shoulder) cm^{-1} whereas species Z has vibrations at 1989, 1965, 1950, 1920, and 1913 (shoulder) cm^{-1}.

All of the spectral estimates exhibit very good signal-to-noise ratios and possess few spectral artifacts (note that the signal intensity of X was particularly low in the catalytic experiments). The spectral estimates of $Rh_4(CO)_{12}$, $(\eta^5\text{-}C_5H_5)Mo(CO)_3H$, and cyclopentene obtained from the reaction spectra are almost identical to the authentic references. The spectral estimate of the nonisolatable complex $C_5H_9CORh(CO)_4$ compares favorably

(16) (a) Chew, W.; Widjaja, E.; Garland, M. *Organometallics* **2002**, *21*, 1882–1990. (b) Widjaja, E.; Li, C.; Garland, M. *Organometallics* **2002**, *21*, 1991–1997. (c) Widjaja, E.; Li, C.; Garland, M. *J. Catal.* **2004**, *223*, 278–289.

(17) Shirt, R.; Garland, M.; Rippin, D. W. T. *Anal. Chim. Acta* **1998**, *374*, 67–91.

(18) (a) Belkova, N. V.; Gutsul, E. I.; Filippov, O. A.; Levina, V. A.; Valyaev, D. A.; Epstein, L. M.; Lledos, A.; Shubina, E. S. *J. Am. Chem. Soc.* **2006**, *128* (11), 3486–3487. (b) Private communication with Shubina, E. S. clarifying the basis sets used.

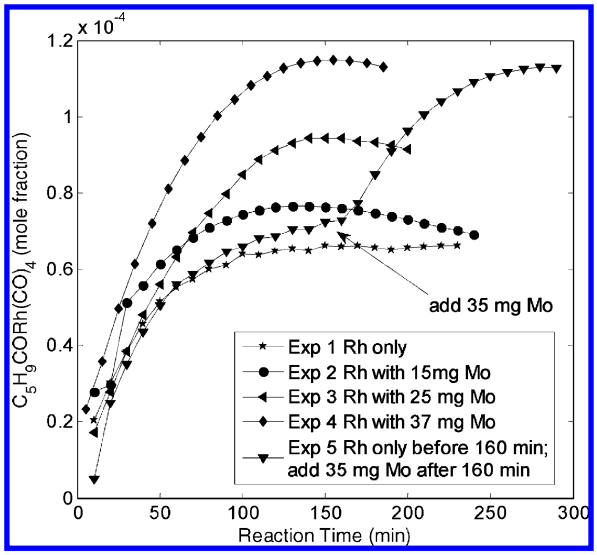

Figure 2. Time-dependent formation of $C_5H_9CORh(CO)_4$ during catalytic hydroformylation experiments starting with $Rh_4(CO)_{12}$ and (η^5-C_5H_5)$Mo(CO)_3H$. The arrow corresponds to the introduction of (η^5-C_5H_5)$Mo(CO)_3H$ in experiment 5.

Table 2. Initial Rates of Formation of $C_5H_9CORh(CO)_4$ (Evaluated for the First 40 Minutes) and the Maximum Yields of $C_5H_9CORh(CO)_4$ as a Function of Mo/Rh Ratio in the Catalytic Hydroformylations

exp no	Mo/Rh loading(mole ratio)	rate of $C_5H_9CORh(CO)_4$ formation(mole fraction /min)	maximum yield of $C_5H_9CORh(CO)_4$(%)
1	0	7.1×10^{-7}	40.1
2	0.82	8.2×10^{-7}	48.2
3	1.36	9.3×10^{-7}	59.2
4	1.88	1.2×10^{-6}	72.5

to previous studies.[9d,e,g,h,19] Since only a rough spectral estimate of the large cluster $Rh_6(CO)_{16}$[20] could be obtained via BTEM analysis, it is apparently present at only trace concentration levels in these experiments. The spectral estimate of new species X appears quite similar to a superposition of the spectra of (η^5-C_5H_5)$Mo(CO)_3H$ and $C_5H_9CORh(CO)_4$ although noticeable band shifts are apparent.

Concentration Profiles. Figure 2 shows the time dependence of the intermediate $C_5H_9CORh(CO)_4$ in the catalytic experiments. As seen in this figure, the base-case pure-rhodium experiment shows (1) a relatively low initial rate of $C_5H_9CORh(CO)_4$ formation and (2) a relatively low yield of $C_5H_9CORh(CO)_4$. In contrast, the experiments with increasing initial concentrations of (η^5-C_5H_5)$Mo(CO)_3H$ show (1) increasingly higher rates of $C_5H_9CORh(CO)_4$ formation and (2) increasingly higher yields of $C_5H_9CORh(CO)_4$. To confirm the unusual effect of (η^5-C_5H_5)$Mo(CO)_3H$ in a different manner, one experiment was started with only $Rh_4(CO)_{12}$ and then at ca. 160 min (η^5-C_5H_5)$Mo(CO)_3H$ was injected. This experiment shows that the late addition of (η^5-C_5H_5)$Mo(CO)_3H$ also results in an increased yield of the $C_5H_9CORh(CO)_4$.

The observations seen in Figure 2 can be further quantified. The initial rate of formation and maximum yields of $C_5H_9CORh(CO)_4$ are presented in Table 2. There is a consistent increase for both the rate of formation as well as the yield of $C_5H_9CORh(CO)_4$ as a function of increasing concentration of (η^5-C_5H_5)$Mo(CO)_3H$.

(19) Garland, M.; Bor, G. *Inorg. Chem.* **1989**, *28* (3), 410–413.
(20) Chini, P. *Chem. Comm.* **1967**, 440–441.

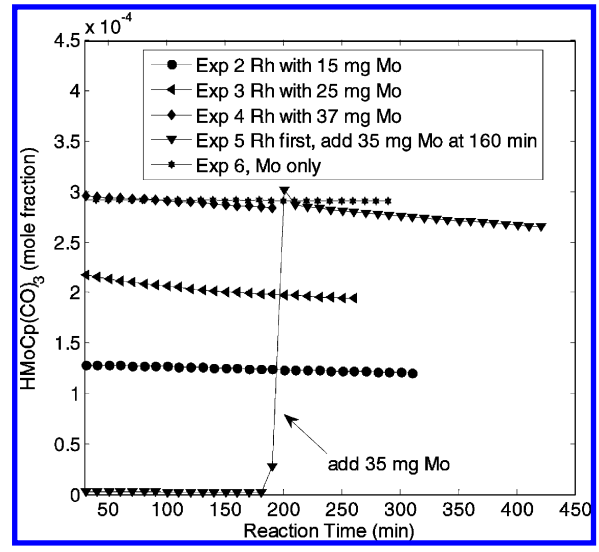

Figure 3. Time-dependent concentrations of (η^5-C_5H_5)$Mo(CO)_3H$ during the catalytic hydroformylation experiments. The arrow corresponds to the introduction of (η^5-C_5H_5)$Mo(CO)_3H$ in experiment 5.

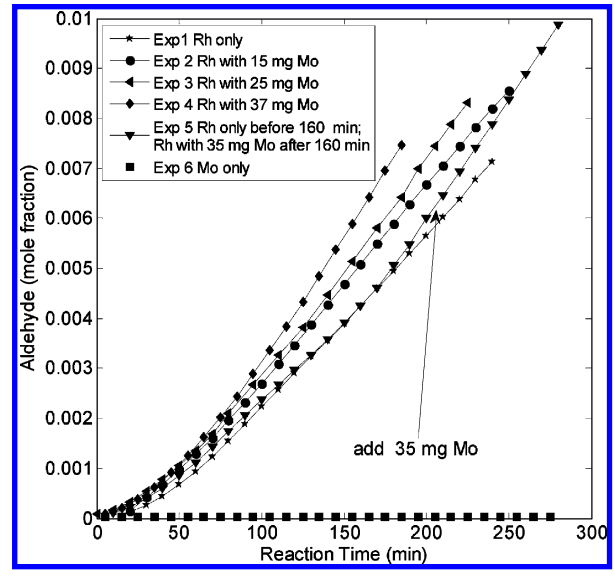

Figure 4. Time-dependent formation of cyclopentane carboxaldehyde in the catalytic hydroformylation experiments. The arrow corresponds to the introduction of (η^5-C_5H_5)$Mo(CO)_3H$ in experiment 5.

Figure 2 provides information not only on the rate of formation and the yield of $C_5H_9CORh(CO)_4$ but also on deactivation phenomenon. Close inspection shows that the concentration of $C_5H_9CORh(CO)_4$ remains constant after 120 min when only $Rh_4(CO)_{12}$ was used as a catalyst precursor, but that the concentration of $C_5H_9CORh(CO)_4$ declines after ca. 120 min when (η^5-C_5H_5)$Mo(CO)_3H$ is present (Exp 5 is an exception due to Mo injection at ca. 160 min).

The time-dependent concentrations of (η^5-C_5H_5)$Mo(CO)_3H$ are shown in Figure 3. As seen in this figure, the concentrations of (η^5-C_5H_5)$Mo(CO)_3H$ are almost constant, although a small decreasing trend is also apparent for the mixed Rh−Mo experiments (Exp 2−5). Since the complex η^5-C_5H_5)$Mo(CO)_3H$ appears stable under hydroformylation conditions (Exp 6), the decreasing trends exhibited in Figure 3 appear to be due to a change in the absorptivity of (η^5-C_5H_5)$Mo(CO)_3H$ (vide infra).

The time-dependent concentrations for the product cyclopentane carboxaldehyde are shown in Figure 4. It is clear from

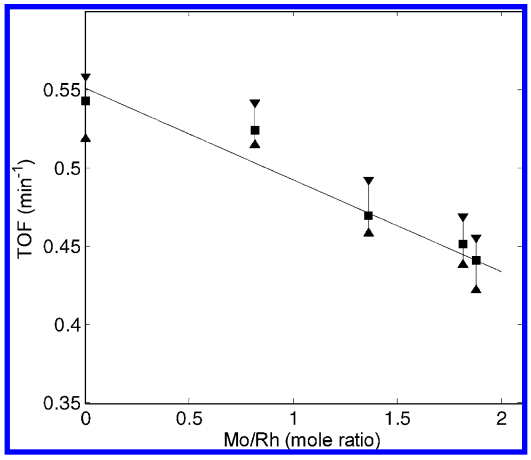

Figure 5. Decrease of TOF with increasing Mo/Rh ratio for the hydroformylation experiments. The error bars correspond to the upper and lower bound for each experiment.

this figure that (1) pure (η^5-C_5H_5)$Mo(CO)_3H$ experiments show no hydroformylation activity and (2) experiments conducted with $Rh_4(CO)_{12}$ and increasing (η^5-C_5H_5)$Mo(CO)_3H$ concentrations result in increased rates of aldehyde formation. For example, at 180 min, the concentrations of aldehyde were 0.0048 mol fraction (Exp 1), 0.0059 mol fraction (Exp 2), 0.0063 mol fraction (Exp 3), and 0.0072 mol fraction (Exp 4).

Analysis of Turnover Frequency. Although the addition of (η^5-C_5H_5)$Mo(CO)_3H$ to the unmodified rhodium catalyzed hydroformylation of cyclopentene increased the rate of formation and yield of $C_5H_9CORh(CO)_4$, it did not increase the turnover frequency of the system. Figure 5 shows the average turnover frequencies for the 5 experiments containing rhodium (see Experimental Section for details), as well as the highest and lowest values. There is a clear and quite significant decrease of TOF with increasing Mo/Rh ratio. This result suggests that the presence of (η^5-C_5H_5)$Mo(CO)_3H$ is interfering with the hydrogenolysis of $C_5H_9CORh(CO)_4$.

Spectral Changes for (η^5-C_5H_5)$Mo(CO)_3H$. BTEM was reapplied to the molybdenium carbonyl range of the catalytic hydroformylation data (Exp 1−6, and latter part of Exp 7). In particular, BTEM analysis was performed separately on (a) the pure (η^5-C_5H_5)$Mo(CO)_3H$ experiment, (b) the first hour, (c) the second hour, (d) the third hour, and (e) the fourth hour of the mixed metal Rh−Mo hydroformylations. The resulting pure component spectral estimates of (η^5-C_5H_5)$Mo(CO)_3H$ for the carbonyl region are shown in Figure 6. There is a change in both the position and the shape of the carbonyl bands. The CO vibrations are shifted to lower wavenumbers. In addition, analysis of different hydroformylation runs provided dramatically different pure component spectral estimates for (η^5-C_5H_5)$Mo(CO)_3H$ (Figure 6, inset). Together, these observations strongly suggest that some sort of solute−solute interaction is occurring. Since the carbonyl vibrational positions systematically change as a function of reaction time as well as Mo−Rh loading, molecular recognition between (η^5-C_5H_5)$Mo(CO)_3H$ and aldehyde and/or $C_5H_9CORh(CO)_4$ appears to occur.

To study any spectral changes in the carbonyl vibration of the aldehyde, spectra from the pure rhodium experiment (Exp 1) were compared to spectra from the Rh/Mo hydroformylations (Exp 2−7). BTEM analysis was performed on both sets to recover the pure component spectrum of aldehyde. The results are shown in Figure 7 where a ca. 2 cm^{-1} shift to lower wavenumbers is observed. Since the main difference is the presence or absence of Mo, the spectral change is consistent with an interaction between (η^5-C_5H_5)$Mo(CO)_3H$ and aldehyde.

BTEM analysis was also performed separately on Exp 1−5 to obtain the pure component spectra of $C_5H_9CORh(CO)_4$ at different Mo loadings. The BTEM estimates of the acyl vibration, with a peak maximum at 1696 cm^{-1}, are shown in Figure 8. The spectral estimate of $C_5H_9CORh(CO)_4$ obtained from Exp 1 (Rh only) differs dramatically from the spectral estimates of $C_5H_9CORh(CO)_4$ obtained from Exp 2−5 (both Rh and Mo present). In addition, BTEM analysis was reapplied to the combined data set from Exp 2−5, and a new acyl vibration is recovered with peak maximum at 1684 cm^{-1}, Figure 8. This result suggests that a solute−solute interaction is

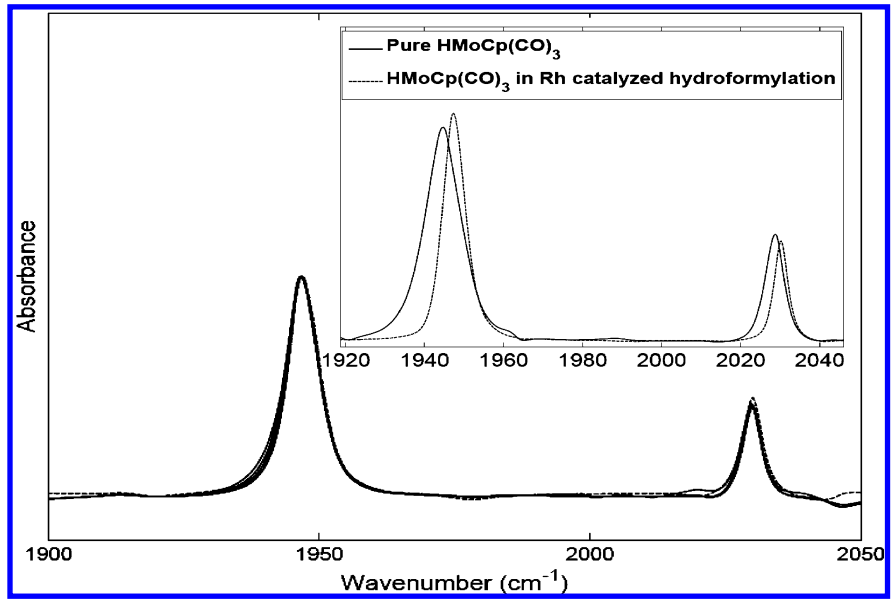

Figure 6. BTEM spectral estimates of (η^5-C_5H_5)$Mo(CO)_3H$ obtained from 5 different spectroscopic data sets in a time series analysis of one hydroformylation experiment. There is a continuous shift to lower wavenumbers for both the bands at 2030 and 1947 cm^{-1} at increased time (also increased aldehyde concentration). (Inset) Large changes in BTEM spectral estimates observed for (η^5-C_5H_5)$Mo(CO)_3H$ between different experimental runs.

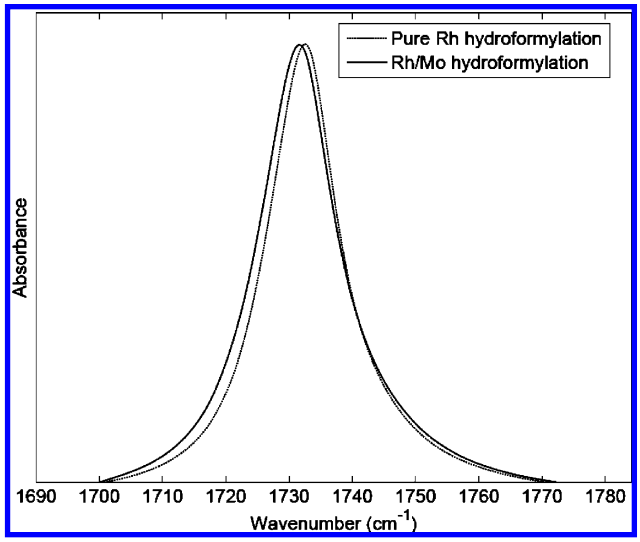

Figure 7. BTEM spectral estimates of aldehyde obtained from catalytic runs Exp 1 (pure Rh) and Exp 2−7 (Rh and Mo).

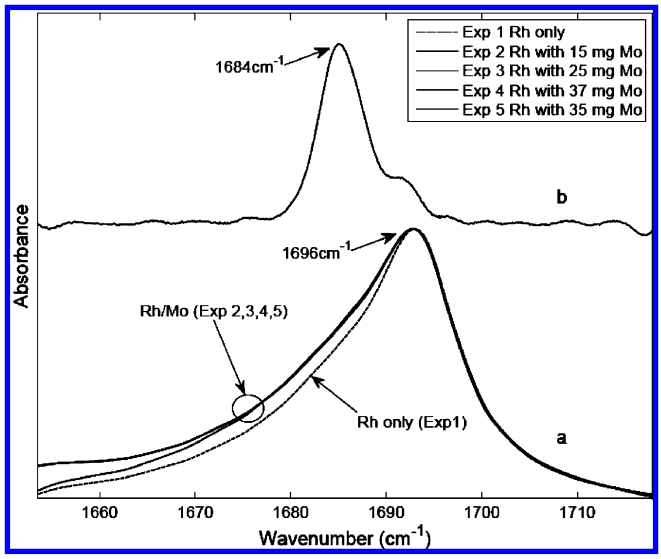

Figure 8. (a) Normalized BTEM spectral estimates of the acyl vibration centered at 1696 cm^{-1} obtained independently for Exp 1−5. (b) BTEM spectral estimate of the acyl vibration centered at 1684 cm^{-1} obtained from the combined data from Exp 2−5. The slightly uneven baseline in the recovered pure component spectrum (b) is due to the relatively low intensity of the new signal.

occurring, in this case, between $(\eta^5\text{-}C_5H_5)Mo(CO)_3H$ and $C_5H_9CORh(CO)_4$.

Determination of Interaction Volume. Independent experiments were conducted on *n*-hexane solutions of $(\eta^5\text{-}C_5H_5)Mo(CO)_3H$ and cyclopentane carboxaldehyde, using in situ FTIR spectroscopy and online density measurements (see Supporting Information). The purpose of these experiments was to determine volumes of interaction v_{11}, self-association of $(\eta^5\text{-}C_5H_5)Mo(CO)_3H$; v_{22}, self-association of cyclopentane carboxaldehyde; and v_{12}, interaction between $(\eta^5\text{-}C_5H_5)Mo(CO)_3H$ and cyclopentane carboxaldehyde. The results presented in Table 3 suggest that (a) there is negligible self-association of $(\eta^5\text{-}C_5H_5)Mo(CO)_3H$, (b) there is measurable self-association of cyclopentane carboxaldehyde, and (c) the volume of interaction between $(\eta^5\text{-}C_5H_5)Mo(CO)_3H$ and cyclopentane carboxaldehyde is very substantial—it is an order of magnitude greater than the self-association of aldehyde. Moreover, the *P*-value tests (and specifically *P*-values below 0.05) provide confirmation of

Table 3. Experimentally Determined Homotactic (v_{ii}) and Heterotactic (v_{ij}) Volumetric Interaction Coefficients for the Solutes $(\eta^5\text{-}C_5H_5)Mo(CO)_3H$ (1) and Cyclopentane Carboxaldehyde (2) in *n*-Hexane under 0.1 MPa Argon at 298 K

solute-i/solute-j	volumetric interaction coefficient, v_{ij}	*P* value
1/1	105.2 ± 1238.5	0.9332
2/2	−62.9 ± 19.6	0.0046
1/2	−817.3 ± 351.6	0.0313

statistical significance. Accordingly, the *P*-values 0.0046 and 0.0313 associated with v_{22} and v_{12}, respectively, confirm that aldehyde−aldehyde and aldehyde−$(\eta^5\text{-}C_5H_5)Mo(CO)_3H$ interactions indeed exist.[17]

DFT Spectral Predictions for Interactions. DFT calculations were performed to (1) better understand the changes observed in the experimental spectra as well as the apparent decrease in the concentration of $(\eta^5\text{-}C_5H_5)Mo(CO)_3H$ (Figure 3) and (2) ultimately better understand the basis for the pronounced decrease in TOF with increasing molybdenum loadings (Figure 5). Accordingly, optimized geometries and IR spectral predictions were carried out for $(\eta^5\text{-}C_5H_5)Mo(CO)_3H$, $C_5H_9CORh(CO)_4$ and cyclopentane carboxaldehyde as well as a variety of different hydrogen bonding scenarios between these species.

The experimental results presented in Figure 6 show that significant spectral changes in the terminal CO vibrations of $(\eta^5\text{-}C_5H_5)Mo(CO)_3H$ occur. Furthermore, these changes correlate with reaction time and hence increasing aldehyde concentration. Accordingly, DFT calculations were performed on $(\eta^5\text{-}C_5H_5)Mo(CO)_3H$ and two different $(\eta^5\text{-}C_5H_5)Mo(CO)_3H$-aldehyde complexes. One of the complexes involved hydrogen bonding of the type Mo−H···O═C and one involved hydrogen bonding through the Cp ring, that is, C_5H_4−H···O═C (Please refer to Supporting Information for details).

Figure 9 shows the optimized geometry as well the spectral prediction for the $(\eta^5\text{-}C_5H_5)Mo(CO)_3H$-aldehyde complex where hydrogen bonding of the type C_5H_4−H···O═C occurs (bond length 2.22 Ångstrom). A ca. 2 wavenumber shift to lower wavenumbers as well as a decrease in the intensity is seen for the bands at both 1947 and 2030 cm^{-1} and little or no change is predicted for the Mo−H vibration at 1820 cm^{-1}. The first two predictions are certainly consistent with the experimental

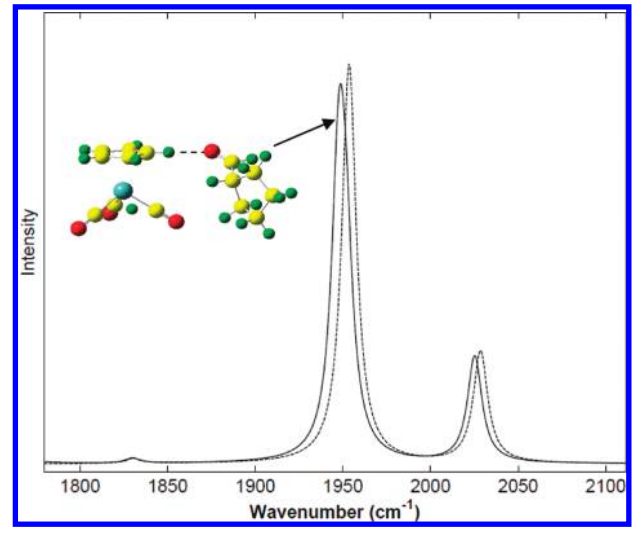

Figure 9. DFT spectral predictions for $(\eta^5\text{-}C_5H_5)Mo(CO)_3H$ (dashed line) and its hydrogen bonded complex (solid line) with aldehyde. The optimized geometry for hydrogen bonding through the Cp ring is also provided.

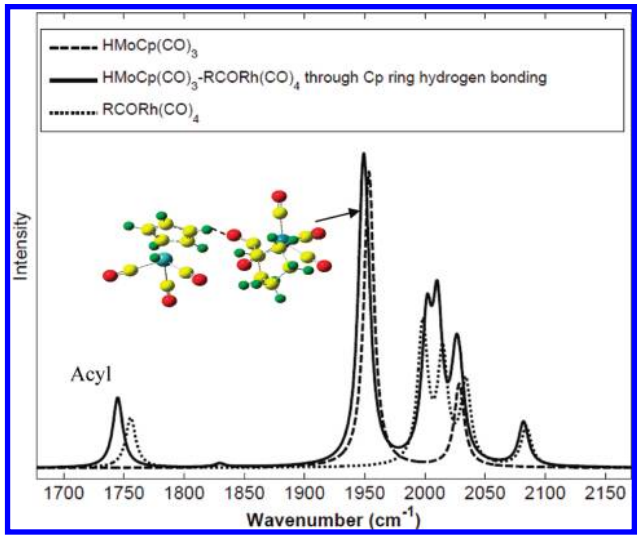

Figure 10. DFT spectral predictions for $C_5H_9CORh(CO)_4$ and its hydrogen bonded complex with $(\eta^5\text{-}C_5H_5)Mo(CO)_3H$. The optimized geometry for hydrogen bonding through the Cp ring is also provided.

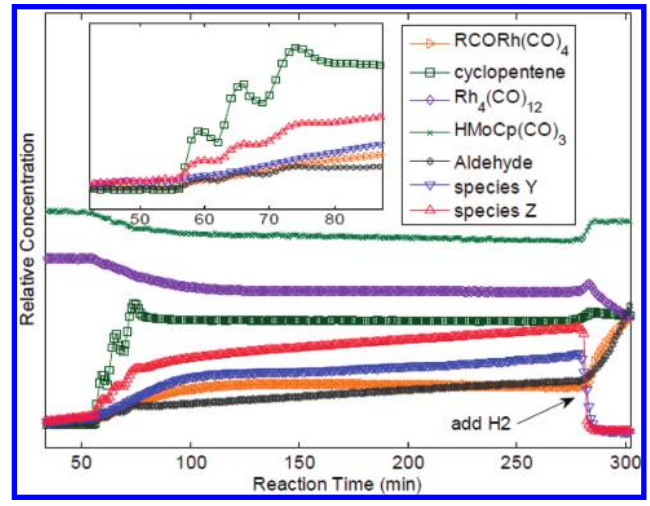

Figure 11. Relative concentration profiles of the primary solutes from Exp 8 in the stoichiometric hydroformylation of cyclopentene starting with the complexes $Rh_4(CO)_{12}$ and $(\eta^5\text{-}C_5H_5)Mo(CO)_3H$. (Inset) Window clarification that alkene additions were performed at ca. 55, 60, and 70 min. Hydrogen was added to the system at 280 min to initiate the catalytic hydroformylation.

observations in Figure 6 (the third prediction is quite difficult to confirm due to the very weak experimental absorptivity of the Mo−H vibration).

Also, the DFT calculations indicate that the complex involving hydrogen bonding through the Cp ring provided the lower free energy (see Supporting Information). In addition, hydrogen bonding through Mo−H···O═C is predicted to split the band at 2030 cm^{-1} significantly, and this is not seen experimentally.

The experimental results presented in Figure 7 showed that spectral changes in the CO vibration of cyclopentane carboxaldehyde occurred with increasing $(\eta^5\text{-}C_5H_5)Mo(CO)_3H$ loading. A shift to lower wavenumbers for C═O was predicted by DFT for both of the two hydrogen bonding scenarios considered between aldehyde and $(\eta^5\text{-}C_5H_5)Mo(CO)_3H$. The shift to a lower wavenumber is consistent with the decrease in C═O bond order upon hydrogen bonding.

The experimental results presented in Figure 8 showed a marked spectral change in the C═O vibration of $C_5H_9CORh(CO)_4$ when $(\eta^5\text{-}C_5H_5)Mo(CO)_3H$ was present in solution. Accordingly, DFT calculations were performed on $C_5H_9CORh(CO)_4$ and two different $(\eta^5\text{-}C_5H_5)Mo(CO)_3H{-}C_5H_9CORh(CO)_4$ complexes. One of the complexes involved hydrogen bonding through Mo−H···O═C and one involved hydrogen bonding through the Cp ring, that is, $C_5H_4{-}H\cdots O{=}C$ (please refer to Supporting Information for details).

Figure 10 shows the DFT predicted spectra of $(\eta^5\text{-}C_5H_5)Mo(CO)_3H$ and $C_5H_9CORh(CO)_4$. The former DFT spectrum almost matches the experimental measurement. Although the latter DFT spectrum shows very accurate relative band intensities, there are noticeable wavenumber shifts from the experimental measurements (see Figure 1). In addition, the optimized geometry for the $(\eta^5\text{-}C_5H_5)Mo(CO)_3H{-}C_5H_9CORh(CO)_4$ complex as well as the DFT spectrum are shown in Figure 10, where hydrogen bonding of the type $C_5H_4{-}H\cdots O{=}C$ occurs (bond length 2.32 Ångstrom). Again, the most intense carbonyl band for the molybdenium at 1947 cm^{-1} is shifted to lower wavenumbers. Also, the acyl vibration is shifted ca. 12 cm^{-1} to lower wavenumbers, which is in agreement with the experimentally observed difference in Figure 8. Taking into consideration (1) that the BTEM spectral estimate of new species X appears quite similar to a superposition of the spectra of $(\eta^5\text{-}C_5H_5)Mo(CO)_3H$ and $C_5H_9CORh(CO)_4$ (see Figure 1) and (2) that the experimental and DFT predicted spectral shifts for the Mo−CO and acyl moiety are consistent, the new species X is assigned to the weak hydrogen bonded complex $(\eta^5\text{-}C_5H_5)Mo(CO)_3H{-}C_5H_9CO\text{-}Rh(CO)_4$ where hydrogen bonding of the type $C_5H_4{-}H\cdots O{=}C$ occurs.

The complex involving hydrogen bonding through the Cp ring provided the lowest free energy in the DFT calculations. The DFT prediction for the complex with bonding through Mo−H···O═C shows a split for the band at 2030 cm^{-1} (see Supporting Information for both issues). Therefore, hydrogen bonding through the Cp ring to $C_5H_9CORh(CO)_4$ appears to be the primary scenario.

The DFT predictions shown in Figures 9 and 10 both indicate a decrease in the absorptivities at 1947 and 2030 cm^{-1}, when hydrogen bonding is occurring between $(\eta^5\text{-}C_5H_5)Mo(CO)_3H$ and aldehyde or $C_5H_9CORh(CO)_4$. Consequently, a least-squares fit of the reference spectra for $(\eta^5\text{-}C_5H_5)Mo(CO)_3H$ onto the reaction spectra will not be as precise when more and more hydrogen bonding occurs. This mis-match will result in an apparent decrease in the $(\eta^5\text{-}C_5H_5)Mo(CO)_3H$ concentration with time. This is precisely the effect that is seen in Figure 3.

Stoichiometric Hydroformylation. Pino et al were apparently the first to demonstrate the possibility of stoichiometric hydroformylation of alkenes, by reacting $Co_2(CO)_8$, H_2, alkene to produce aldehyde and $Co_4(CO)_{12}$.[21] Subsequently, Chini et al showed a similar stoichiometric hydroformylation with rhodium at 293K, using 3 $Rh_4(CO)_{12}$ + 4 H_2 + 4 alkene to give 4 aldehyde and 2 $Rh_6(CO)_{16}$.[22] In both cases, the starting metal carbonyls provide the needed CO for the aldehyde product.

The first half of Exp 7 and 8 represents a new variation on the theme of stoichiometric hydroformylation. In this new variation, the starting metal hydride provides all the needed hydrogen for the aldehyde product. Figure 11 shows that the reaction was very fast upon addition of alkene to the system, then appeared to equilibrate, as suggested by the sustained and

(21) Pino, P.; Ercoli, R.; Calderazzo, F. *Chim. Ind.* **1955**, *37*, 782.
(22) Chini, P.; Martinengo, S.; Garlaschelli, G. *J. Chem. Soc., Chem. Comm.* **1972**, 709.

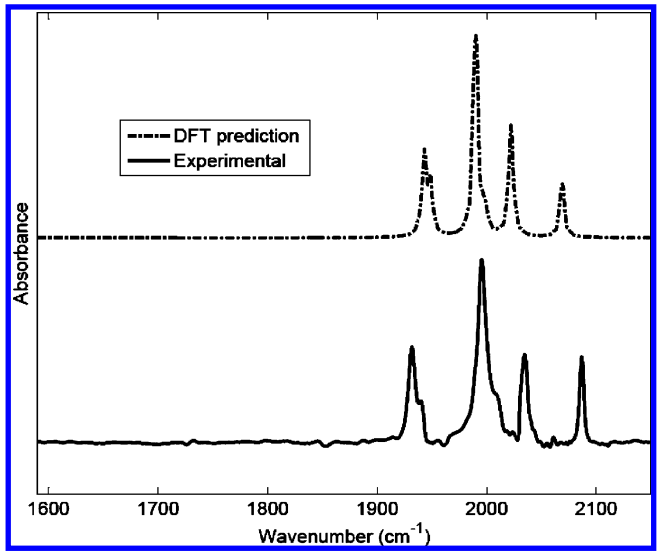

Figure 12. Comparison of the BTEM spectral estimate and DFT-predicted spectrum of (η^5-C_5H_5)$Mo(CO)_3$-$Rh(CO)_4$.

simultaneous presence of the metal carbonyls $Rh_4(CO)_{12}$, (η^5-C_5H_5)$Mo(CO)_3H$, $RCORh(CO)_4$, and new Species Y and Z, as well as aldehyde. In Exp 8, multiple perturbations of alkene were introduced, and the species Z showed an immediate and pronounced increase in concentration upon each addition of cyclopentene to the system, and a new equilibrium state was rapidly established as seen by the step-function increases in aldehyde concentration.

Figure 11 also shows that upon addition of molecular hydrogen to the system at ca. 280 min, catalytic hydroformylation commenced very quickly and the Species Y and Z very rapidly disappeared, giving rise to increased concentrations of both $Rh_4(CO)_{12}$ and (η^5-C_5H_5)$Mo(CO)_3H$. This indicates that the species Y and Z can rapidly activate molecular hydrogen under high CO pressure and that Y and Z are heterobimetallic.

Given the precedence of other heterobimetallic dinuclear complexes to readily activate molecular hydrogen under high CO pressures, particular $CoMo(CO)_7Cp$,[23c] $CoRh(CO)_7$[23a,b] and $RhRe(CO)_9$,[9g] DFT calculations were performed on numerous possible heterobimetallic Rh−Mo complexes to identify species Y and Z. In particular, very good agreement was obtained between the BTEM spectral estimate of species Y and the DFT predicted spectrum of (η^5-C_5H_5)$Mo(CO)_3$-$Rh(CO)_4$ (Figure 12 and Supporting Information). It can be mentioned that this species has a spectrum similar to the known species (η^5-C_5H_5)$Mo(CO)_3$-$Co(CO)_4$ and that the DFT-predicted geometry (η^5-C_5H_5)$Mo(CO)_3$-$Rh(CO)_4$ is similar to the determined crystal structure of (η^5-RC_5H_4)$Mo(CO)_3$-$Co(CO)_4$.[23c,d]

The BTEM spectral estimate of species Z indicates that (i) there are no bridging CO and (ii) the symmetry at Mo has been dramatically changed as evidenced by the shift in the highest C−O vibration from 2030 to 1989 cm^{-1}. In previous studies of the Mo−Co complexes,[23c] both (η^5-C_5H_5)$Mo(CO)_3$-$Co(CO)_3L$ and (η^5-C_5H_5)$Mo(CO)_2L$-$Co(CO)_3L$ where L = solvent, P(n-Bu)$_3$ have been identified. The former species has its highest C−O vibration at 2024 cm^{-1}, and the latter has its highest C−O vibration at 1993 or 1990 cm^{-1} depending on the isomer considered. Since the species Z appears to be in equilibrium exchange with $RhMo(CO)_7$(η^5-C_5H_5) and alkene (see Figure 11), we tentatively assign the stoichiometry $RhMo(CO)_{7-y}$(η^5-C_5H_5)L_y where y = 1 or 2, and L = (π-C_5H_8) to species Z. Numerous DFT calculations were attempted for isomers of (η^5-C_5H_5)Mo-

Scheme 1. Possible Set of Reactions Consistent with Stoichiometric Hydroformylation Starting with $Rh_4(CO)_{12}$ and (η^5-C_5H_5)$Mo(CO)_3H$

$$Rh_4(CO)_{12} + 2(\eta^5\text{-}C_5H_5)Mo(CO)_3H + 4CO \rightarrow 2HRh(CO)_4 + 2RhMo(CO)_7(\eta^5\text{-}C_5H_5) \quad (1)$$

$$2HRh(CO)_4 + 2\text{alkene} + 2CO \rightarrow 2RCORh(CO)_4 \quad (2)$$

$$2RCORh(CO)_4 + 2(\eta^5\text{-}C_5H_5)Mo(CO)_3H \rightarrow 2\text{aldehyde} + 2RhMo(CO)_7(\eta^5\text{-}C_5H_5) \quad (3)$$

($CO)_3$-$Rh(CO)_3L$ and (η^5-C_5H_5)$Mo(CO)_2L$-$Rh(CO)_3L$ where L = (π-C_5H_8); however, none of the DFT-predicted spectra closely matched the BTEM spectral estimate.

The presence of detectable quantities of $RCORh(CO)_4$ in the stoichiometric hydroformylation indicates that the formation of a rhodium hydride occurred. One possible set of stoichiometric reactions, which would be consistent with both the formation of a rhodium hydride and the formation $RCORh(CO)_4$ is given in Scheme 1, where the apparent overall reaction is $Rh_4(CO)_{12}$ + 4 (η^5-C_5H_5)$Mo(CO)_3H$ + 6 CO + 2 alkene → 2 aldehyde and 4 $RhMo(CO)_7$(η^5-C_5H_5).

The stochiometric hydroformylation results also help to clarify the issue of increased rate and yield of $RCORh(CO)_4$, which was presented earlier in Figure 2 and Table 2 for the catalytic experiments. Indeed, eqs 1 and 2 of Scheme 1 represent a plausible route for the formation of $RCORh(CO)_4$ arising from the attack of (η^5-C_5H_5)$Mo(CO)_3H$ on $Rh_4(CO)_{12}$. The issue of metal hydride assisted conversion of metal carbonyl clusters has been discussed for other cases elsewhere.[9d−h]

Catalytic Binuclear Elimination. Since the stoichiometric hydroformylation resulted in the formation of the heterobimetallic complex (η^5-C_5H_5)$Mo(CO)_3$-$Rh(CO)_4$, and since (η^5-C_5H_5)$Mo(CO)_3$-$Rh(CO)_4$ readily activates molecular hydrogen, a catalytic binuclear elimination reaction is probably occurring in the catalytic system. To confirm this possibility, a deutero-formylation (Exp 9) was performed. For the initial 320 min, the pure rhodium deutero-formylation resulted in d-aldehyde $C\underline{D}OCDHCH_2C(CH_3)_3$ with a CO vibration at 1723 cm^{-1}. In this experiment, using the more reactive 3,3-dimethylbut-1-ene as substrate, ca. 90% conversion of $Rh_4(CO)_{12}$ to $RCORh(CO)_4$ occurred in these initial 320 min. (η^5-C_5H_5)$Mo(CO)_3H$ was then added to the system. The new FTIR spectra taken immediately thereafter indicated the presence of 2 CO vibrations centered at 1723 and 1733 cm^{-1}. This observation confirms the formation of $RC\underline{H}O$ and the role of (η^5-C_5H_5)$Mo(CO)_3H$ as the hydrogen source.

In addition, mass balances were performed. At 320 min, the amount of $RCORh(CO)_4$ present was ca. 9.7 × 10^{-5} moles, while the $Rh_4(CO)_{12}$ was ca. 2.0 × 10^{-6} moles. Upon addition of (η^5-C_5H_5)$Mo(CO)_3H$, the product $RC\underline{H}O$ was formed at a rather high rate. The total amount of $RC\underline{H}O$ produced was ca. 1.5 × 10^{-4} moles, in close agreement with the 1.7 × 10^{-4} moles of (η^5-C_5H_5)$Mo(CO)_3H$ added at 320 min. In Table 4, three synthetic pathways are considered for the formation of aldehyde from (η^5-C_5H_5)$Mo(CO)_3H$. The close correspondence between the moles of $RC\underline{H}O$ formed and the moles of (η^5-C_5H_5)$Mo(CO)_3H$ introduced confirms the presence of catalytic binuclear elimination in this bimetallic system. However, the initial rate of $RC\underline{H}O$ formation versus the rate of $RC\underline{D}O$ formation suggests that only ca. 10% of the aldehyde formation occurs via a CBER mechanism.

Discussion

General. The in situ measured solute concentrations provided a number of important observations. For example, the rate of

Table 4. Possible Synthetic Pathways for the Formation of Aldehyde from $(\eta^5\text{-}C_5H_5)Mo(CO)_3H$ in the Catalytic Deutero-Formylation (Exp 9)

reaction	type of aldehyde produced	moles RCHO produced per $(\eta^5\text{-}C_5\underline{H}_5)Mo(CO)_3H$
1. $Rh_4(CO)_{12} + 4(\eta^5\text{-}C_5H_5)Mo(CO)_3H + 6\,CO + 2$ alkene → 2 aldehyde and $4RhMo(CO)_7(\eta^5\text{-}C_5H_5)$. (Scheme 1)	$C\underline{H}OCH_2CH_2C(CH_3)_3$	1/2
2a. $Rh_4(CO)_{12} + 2(\eta^5\text{-}C_5H_5)Mo(CO)_3H + 6CO + 2$ alkene → $2(CH_3)_3CCH_2CH_2CORh(CO)_4 + 2\,RhMo(CO)_7(\eta^5\text{-}C_5H_5)$	$C\underline{D}OCH_2CH_2C(CH_3)_3$	0
2b. $2(CH_3)_3CCH_2CH_2CORh(CO)_4 + 2D_2$ → 2 aldehyde + $2\,DRh(CO)_4$		
3. $(CH_3)_3CCH_2CDHCORh(CO)_4 + (\eta^5\text{-}C_5H_5)Mo(CO)_3H$ → aldehyde + $RhMo(CO)_7(\eta^5\text{-}C_5H_5)$	$C\underline{H}OCDHCH_2C(CH_3)_3$	1

formation and yield of $C_5H_9CORh(CO)_4$ as well as the increased rate of aldehyde formation as a function of molybdenum loading both indicate a positive effect of $(\eta^5\text{-}C_5H_5)Mo(CO)_3H$ on the rhodium catalyzed hydroformylation of cyclopentene. However, the decreasing turnover frequencies with increasing molybdenum loading strongly suggested that $(\eta^5\text{-}C_5H_5)Mo(CO)_3H$ plays an inhibitory role and reduces the efficiency of the catalytic cycle. In addition, the decrease in $C_5H_9CORh(CO)_4$ concentrations at long reaction times when $(\eta^5\text{-}C_5H_5)Mo(CO)_3H$ is present, but not when $Rh_4(CO)_{12}$ is used alone, is an observation that warrants further explanation.

The changes observed for the in situ measured band positions and band shapes for $(\eta^5\text{-}C_5H_5)Mo(CO)_3H$, $C_5H_9CORh(CO)_4$, and cyclopentane carboxaldehyde suggested the existence of $(\eta^5\text{-}C_5H_5)Mo(CO)_3H$-cyclopentane carboxaldehyde and $(\eta^5\text{-}C_5H_5)Mo(CO)_3H{-}C_5H_9CORh(CO)_4$ solute−solute interactions during the catalysis. The spectroscopic changes in the acyl vibration of $C_5H_9CORh(CO)_4$ were the most significant (Figure 8). Independent physicochemical measurements on solutions of $(\eta^5\text{-}C_5H_5)Mo(CO)_3H$ and cyclopentane carboxaldehyde confirmed that $(\eta^5\text{-}C_5H_5)Mo(CO)_3H$-cyclopentane carboxaldehyde interactions are quite significant.

The origin of the solute−solute interactions was further examined using DFT. It was concluded that interaction through the Cp ring on molybdenum to the organic carbonyl groups of aldehyde and $C_5H_9CORh(CO)_4$ are the most likely interactions. This does not negate the possibility of some hydrogen bonding of the type Mo−H···O═C; however, hydrogen bonding of the type $C_5H_4{-}H\cdots O{=}C$ is consistent with all of the available experimental results. Given the widespread use of metallocenes in organic syntheses,[24] the present results suggest that similar Cp hydrogen-bonding interactions might be influencing selectivity and activity patterns in other catalytic systems.

The stoichiometric hydroformylations allowed the observation of two further heterobimetallic species, namely, $(\eta^5\text{-}C_5H_5)Mo(CO)_3\text{-}Rh(CO)_4$ and species Z. In addition, it was found that these species can rapidly activate molecular hydrogen under significant CO partial pressure. The existence of the former species, together with the labeled hydroformylation experiment (Exp 9), confirms that catalytic binuclear elimination is occurring in this Rh−Mo system; however, this contribution is not the major synthetic route for aldehyde formation.

Therefore, in summary, the present heterobimetallic hydroformylation is quite complex, since it involves concurrent inhibitory effects due to hydrogen bonding and synergistic effects, that is, $(\eta^5\text{-}C_5H_5)Mo(CO)_3H$ assisted cluster fragmentation and catalytic binuclear elimination.

Crystallographic Support. Independent support for an interaction of the type $C_5H_4{-}H\cdots O{=}C$ can be obtained from crystallographic databases. A search of the Cambridge Structural Database (CSD) revealed numerous crystal structures where the H---O interatomic distance (between a $\eta^5\text{-}C_5H_5$ moiety and a C═O) is in a range consistent with some orbital overlap and hydrogen bonding. Table S-8 (Supporting Information) lists 29 structures where a distance of less than 2.40 Å occurs between H on Cp and the O on an organic carbonyl. In addition, Table S-9 (Supporting Information) lists 13 structures where a distance of less than 2.40 Å occurs between H on Cp and the O on an organic carbonyl moiety in an organometallic compound. It can be noted that there are many other similar structures in the CSD with somewhat longer H---O distances as well. This solid-state database search further supports the conclusions reached in the present liquid-phase catalytic experiments.

It should be noted that crystallographic data has been extensively used to support hydrogen bonding hypotheses. Of particular relevance is the work on organometallic systems, and especially hydrogen bonding of the type M-H---O═C and $C_5H_4{-}H\cdots O{=}C$ in metallocene systems where the C═O is a terminal or bridged metal carbonyl.[25] It has been noted elsewhere that, in many cases, hydrogen bonding of the type $C_5H_4{-}H\cdots O{=}C$ is the predominate scenario in the solid state.[26]

$(\eta^5\text{-}C_5H_5)Mo(CO)_3H$ and $C_5H_9CORh(CO)_4$ Interactions and TOF. It was concluded that hydrogen bonding of the type $C_5H_4{-}H\cdots O{=}C$ between $(\eta^5\text{-}C_5H_5)Mo(CO)_3H$ and C_5H_9CORh-

(23) (a) Horvath, I.; Garland, M.; Bor, G.; Pino, P. *J. Organomet. Chem.* **1988**, *358*, C17–C22. (b) Garland, M.; Pino, P. *Organometallics* **1990**, *9*, 1943–1949. (c) Kovacs, I.; Sisak, A.; Ungvary, F.; Marko, L. *Organometallics* **1989**, *8*, 1873–1877. (e) Song, X.; Brown, T. *Inorg. Chem.* **1995**, *34*, 3220–3231. (d) Song, L.; Shen, J.; Wang, J.; Hu, Q.; Wang, R.; Wang, H. *Polyhedron* **1994**, *13*, 3235–3241.

(24) (a) Marks, T. J. *Chem. Rev.* **2000**, *100* (4), 1391–1434. (b) *Metallocenes in Regio- and Stereoselective Synthesis*; Takahasi, T., Ed.; Springer: New York, 2005.

(25) (a) Braga, D.; Grepioni, F.; Biradha, K.; Pedireddi, V. R.; Desiraju, G. R. *J. Am. Chem. Soc.* **1995**, *117* (11), 3156–66. (b) Braga, D.; Grepioni, F. *Acc. Chem. Res.* **1997**, *30* (2), 81–87. (c) Choi, J. C.; Pulling, M. E.; Smith, D. M.; Norton, R. J. *J. Am. Chem. Soc.* **2008**, *130*, 4250–4252.

(26) Braga, D.; Grepioni, F.; Tedesco, E.; Biradha, K.; Desiraju, G. R. *Organometallics* **1996**, *15* (12), 2692–2699.

Scheme 2. Proposed Reaction Topology for Simultaneous (1) Rhodium-Catalyzed Hydroformylation, (2) Inhibition of the Rhodium Catalysis Due to the Presence of $(\eta^5\text{-}C_5H_5)Mo(CO)_3H-C_5H_9CORh(CO)_4$, and (3) Rh−Mo CBER in Rh−Mo Bimetallic Catalysis[a]

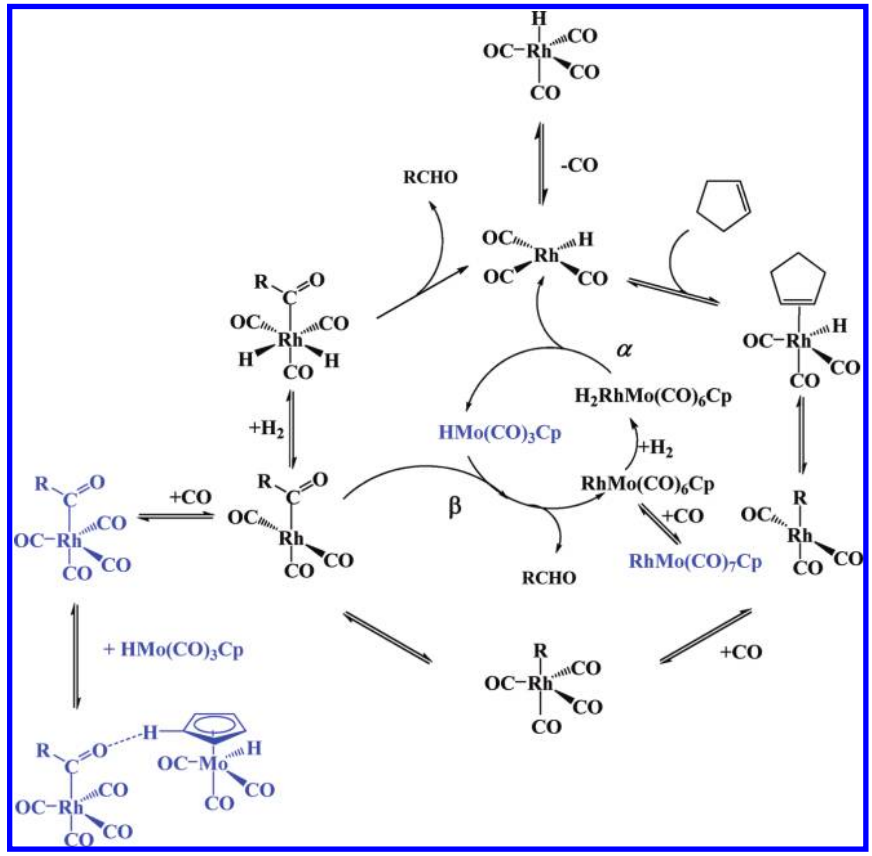

[a] Blue highlighted species are observable organometallics in the system.

$(CO)_4$ exists. The existence of a weak heterobimetallic hydrogen-bonded complex $(\eta^5\text{-}C_5H_5)Mo(CO)_3H-C_5H_9CORh(CO)_4$ during catalysis has a number of consequences. First, a large portion of space around the rhodium atom in $C_5H_9CORh(CO)_4$ is effectively shielded. Second, the formation of the complex should (a) interfere with effective dissociation of a terminal CO from Rh, (b) hinder the approach of molecular hydrogen to the resulting coordinatively unsaturated $\{C_5H_9CORh(CO)_3\}$, and possibly (c) alter the activation energies for oxidative addition of H_2 to rhodium as well as the subsequent hydrogenolysis of the Rh−acyl bond. The first two situations, a and b, would certainly result in a marked decrease in the experimental TOF (as observed in Figure 5) for the catalytic cycle. The main experimental conclusion is that the solute−solute interaction between $(\eta^5\text{-}C_5H_5)Mo(CO)_3H$ and $C_5H_9CORh(CO)_4$ results in the formation of the hydrogen bonded complex $(\eta^5\text{-}C_5H_5)Mo(CO)_3H-C_5H_9CORh(CO)$ which in turn results in a decrease in the rate of hydrogen activation and hence a decrease for TOF in the system.

Decreasing $C_5H_9CORh(CO)_4$ Concentrations at Longer Reaction Time. At reaction times greater than ca. 120 min, there is a small decrease in the concentrations of $C_5H_9CORh(CO)_4$ in the bimetallic experiments (Exp 2−4). A relatively straightforward explanation is provided by the increasing aldehyde concentrations. As the aldehyde concentration increases during the course of a hydroformylation experiment, a small net increase in the concentration of a weak $(\eta^5\text{-}C_5H_5)Mo(CO)_3H$−aldehyde complex will result. When this occurs, slightly less free $(\eta^5\text{-}C_5H_5)Mo(CO)_3H$ is available for the $(\eta^5\text{-}C_5H_5)Mo(CO)_3H$-assisted transformation of $Rh_4(CO)_{12}$ to $C_5H_9CORh(CO)_4$. Consequently, the yield of $C_5H_9CORh(CO)_4$ slowly declines with increasing aldehyde concentrations.

Representation of Catalytic System. The results of the catalytic and stoichiometric experiments suggest that the present bimetallic catalytic system consists of (1) a classic rhodium-catalyzed hydroformation, (2) a rhodium-catalyzed hydroformylation that is inhibited by the presence of hydrogen bonding between $RCORh(CO)_4$ and $(\eta^5\text{-}C_5H_5)Mo(CO)_3H$ and (3) a catalytic binuclear elimination reaction involving the slow attack of $(\eta^5\text{-}C_5H_5)Mo(CO)_3H$ on $RCORh(CO)_4$ resulting in a heterobimetallic complex and aldehyde. The heterobimetallic complex then activates molecular hydrogen to reform $HRh(CO)_4$ (hence $RCORh(CO)_4$) and $(\eta^5\text{-}C_5H_5)Mo(CO)_3H$. A representation of these combined effects is shown in Scheme 2.

In Scheme 2, there are two mechanisms for aldehyde formation (the oxidation addition of hydrogen to $RCORh(CO)_3$ and the binuclear elimination step β). However, closer inspection suggests that the heterobimetallic hydrogen-bonded complex $(\eta^5\text{-}C_5H_5)Mo(CO)_3H-C_5H_9CORh(CO)_4$ itself may also be involved in aldehyde formation. For example, the hydrogen-bonded complex may undergo CO dissociation followed by intramolecular hydrogen transfer to cleave the Rh−acyl bond (Scheme 3). Alternatively, the hydrogen-bonded complex may undergo CO dissociation followed by oxidative addition of molecular hydrogen (Scheme 4). From an experimental viewpoint, the β step and Scheme 3 are quite similar, since both begin with the individual mononuclear complexes and result in the heterobimetallic binuclear complex (the only difference being the lack of hydrogen bonding and presence of hydrogen bonding, respectively). Since a least-squares fit of the $(\eta^5\text{-}C_5H_5)Mo(CO)_3H$ spectral region suggests only ca. 10% of the $(\eta^5\text{-}C_5H_5)Mo(CO)_3H$ is hydrogen bonded, Schemes 3 and 4 might contribute little to aldehyde formation if they exist. Further-

Scheme 3. Possible Intramolecular Route for Aldehyde Formation from the Hydrogen-Bonded Heterobimetallic Complex

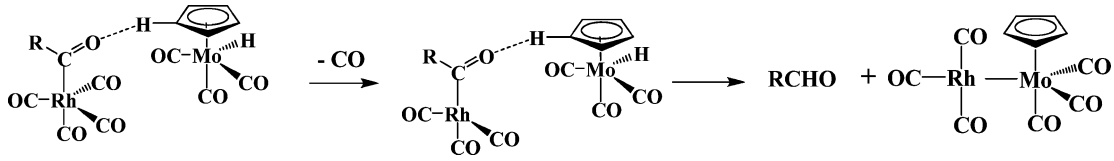

Scheme 4. Possible Hydrogen Addition Route for Aldehyde Formation from the Hydrogen-Bonded Heterobimetallic Complex

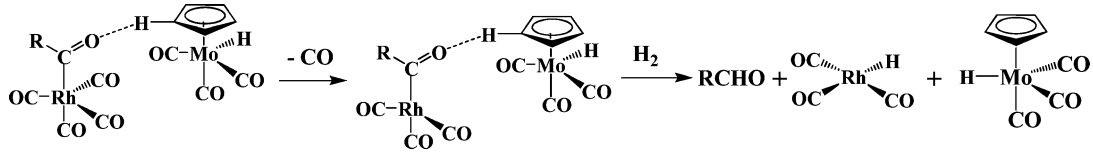

more, Figure 5 clearly shows a *net* decrease in TOF with increased Mo loading (increased hydrogen bonding), and therefore, the *net* effect of the presence of $(\eta^5\text{-}C_5H_5)\text{-}Mo(CO)_3H{-}C_5H_9CORh(CO)_4$ is inhibitory.

A final remark with respect to the thermochemistry of $(\eta^5\text{-}C_5H_5)Mo(CO)_3H{-}C_5H_9CORh(CO)_4$ is useful. Since the experimentally obtained equilibrium conversion was ca. 10%, the experimental Gibbs free energy change corresponds to approximately 4.0 kcal/mol. In contrast, the DFT-predicted free energy changes were slightly greater than 0 kcal/mol (corresponding to ca. 0.01% conversion). This discrepancy appears to be related to the known accuracy/sensitivity of DFT thermochemical calculations, particularly those involving transition metal carbonyls.[27]

Detection of Solute−Solute Interactions During Catalysis—A Possible Future Direction. In the past decade, experimental progress has been made with both 2D Raman spectroscopy and 2D infrared spectroscopy (vibrational equivalents of 2D NMR).[28] In particular, there has been keen interest in the use of these new techniques to directly identify weak and brief intra- and intermolecular interactions, even those involved in solvation. Such interactions are detectable due to the vibrational energy transfer occurring between the moieties involved. Since vibrational spectroscopies are (1) generally very sensitive, with relatively short measurement time, (2) not restricted to the presence/use of any particular isotopes, and therefore applicable to all atom-combinations/moieties present, and (3) normally readily applied to reactive systems, 2D vibration techniques together with signal processing might provide a unique opportunity for identifying subtle molecular interactions in homogeneous catalytic systems. Finally, the combined application of such new and sophisticated in situ spectroscopic techniques, with supporting thermo-physical measurements and first principal calculations might allow considerably greater insight into subtle but important molecular interactions affecting regio-, chemo-, and stereoselective syntheses.

Conclusion

The Rh−Mo catalyzed hydroformylation of cyclopentene exhibits a number of interesting and unusual spectroscopic and kinetic effects. A combination of spectroscopic and kinetic measurements as well as DFT calculations and volume of interaction determinations were used to identify the primary mechanistic reasons behind these effects. In summary, two main mechanistic routes exist for aldehyde formation, and concurrent synergistic and inhibitory effects exist in this heterobimetallic system. Catalytic binuclear elimination is one of the primary synergistic effects, and the heterobimetallic complex $RhMo(CO)_7(\eta^5\text{-}C_5H_5)$ was shown to rapidly active molecular hydrogen. The formation of a heterobimetallic hydrogen-bonded $(\eta^5\text{-}C_5H_5)Mo(CO)_3H{-}C_5H_9CORh(CO)_4$ complex, where hydrogen bonding of the type $C_5H_4{-}H\cdots O{=}C$ occurs, is the primary reason for inhibition and decreased TOFs. The formation of this weak hydrogen-bonded complex decreases the effective rate of hydrogen activation on $C_5H_9CORh(CO)_4$. Hence, the present study shows that quite subtle solute−solute interactions can be indentified during homogeneous catalysis. In addition, the present study also suggests it may be necessary to consider competing effects (synergistic as well as inhibitory) when analyzing the results from complex bimetallic catalytic systems.

Acknowledgment. This work was supported by the Science and Engineering Research Council of A*STAR (Agency for Science, Technology and Research), Singapore. We thank reviewers for their suggestions and thank Professor E. S. Shubina for clarifying the basis sets used in their DFT calculations (ref 18).

Supporting Information Available: Detailed experimental setup; detailed volumetric measurement results; detailed DFT prediction results; detailed Cambridge Structural Database (CSD) analysis; complete ref 8b. This material is available free of charge via the Internet at http://pubs.acs.org.

JA909696B

(27) Proynov, E.; Chermete, H.; Salahub, D. R. *J. Chem. Phy.* **2000**, *113*, 10013–10027.

(28) (a) Mukamei, S.; Piryatinski, A.; Chernyak, V. *Acc. Chem. Res.* **1999**, *32*, 145–154. (b) Tokmakoff, A.; Lang, M. J.; Larsen, D. S.; Fleming, G. R. *Phys. Rev. Lett.* **1997**, *79*, 2702–2705. (c) Hahn, S.; Kwak, K.; Cho, M. *J. Chem. Phy.* **2000**, *112*, 4553–4557. Nagata, Y.; Tanimura, Y. *J. Chem. Phys.* **2006**, *124*, 024508-1–024508-9. (d) Wright, J. C.; Zhao, W.; Murdoch, K. M.; Besemann, D. M.; Condon, N. J.; Meyer, K. A. In *Handbook of Vibrational Spectroscopy*; Chambers, J. M., Griffiths, P. R., Eds.; Wiley: New York, 2002; Vol. 1, pp 853−865.